Electronic supplementary information

Tuning the matrix metalloproteinase-1 degradability of peptide amphiphile nanofibers through supramolecular engineering

Yejiao Shi, [a] Daniela S. Ferreira, [a] Jayati Banerjee, [a] Andrew R. Pickford [b] and Helena S. Azevedo [a] *

[a] School of Engineering and Materials Science & Institute of Bioengineering, Queen Mary, University of London, E1 4NS, UK, E-mail: h.azevedo@qmul.ac.uk
[b] Centre for Enzyme Innovation & School of Biological Sciences, University of Portsmouth, PO1 2DY, UK

* E-mail: h.azevedo@qmul.ac.uk

Contents

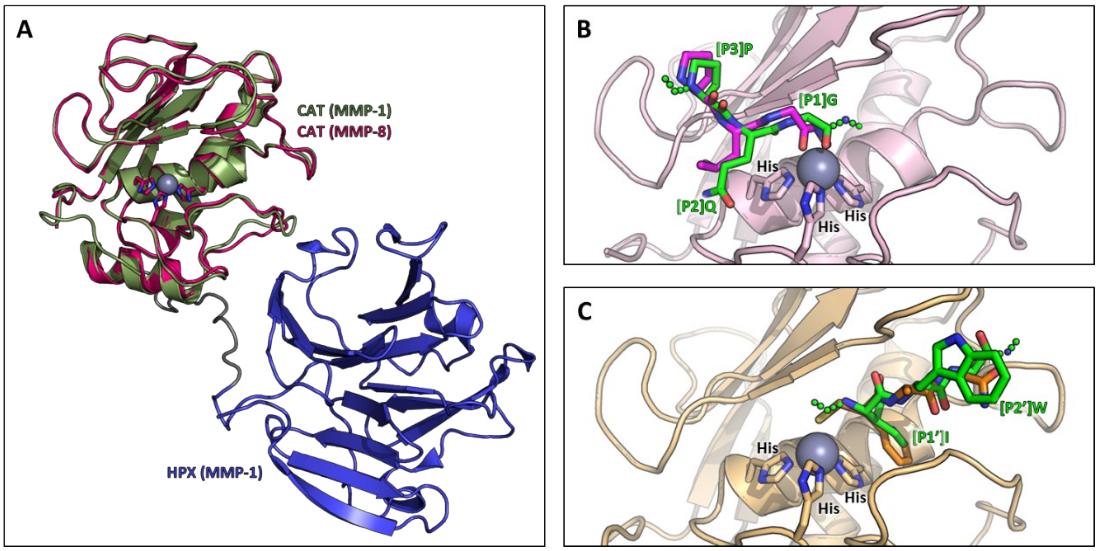

Fig. S1 Templates for modelling of the MMP-1:GPQGIWGQ peptide complex: (**A**) structural homology between the MMP-8 catalytic (CAT) domain (PDB accession code 1JAO) and that of MMP-1 (2CLT). Note that the MMP-8 crystal structure lacks the C-terminal hemopexin (HPX) domain; (**B**) modelling of the [P3]Pro-[P2]Gln-[P1]Gly tripeptide fragment (green) on the crystal structure of MMP-8 (pale pink) in complex with the inhibitor Pro-Leu-Gly-hydroxamate (magenta; 1JAP). The slight displacement of the peptide backbone arises from differential interactions of the active site zinc (grey sphere). In the MMP-8:inhibitor complex, this ion is chelated by the inhibitor's hydroxamate group, but in our model it is chelated by the hydrolyzing water molecule (not shown) that performs a nucleophilic attack on the carbonyl carbon of the scissile peptide bond; (**C**) Modelling of the [P1']Ile-[P2']Trp-[P3']Gly tripeptide fragment (green) on the crystal structure of MMP-8 (pale orange) in complex with the inhibitor 3-mercapto-2-benzylpropanoyl-Ala-Gly-NH_2 (orange; 1JAO). The backbone atoms of [P3']Gly lie directly behind the sidechain of [P2']Trp and, hence, are not labelled.

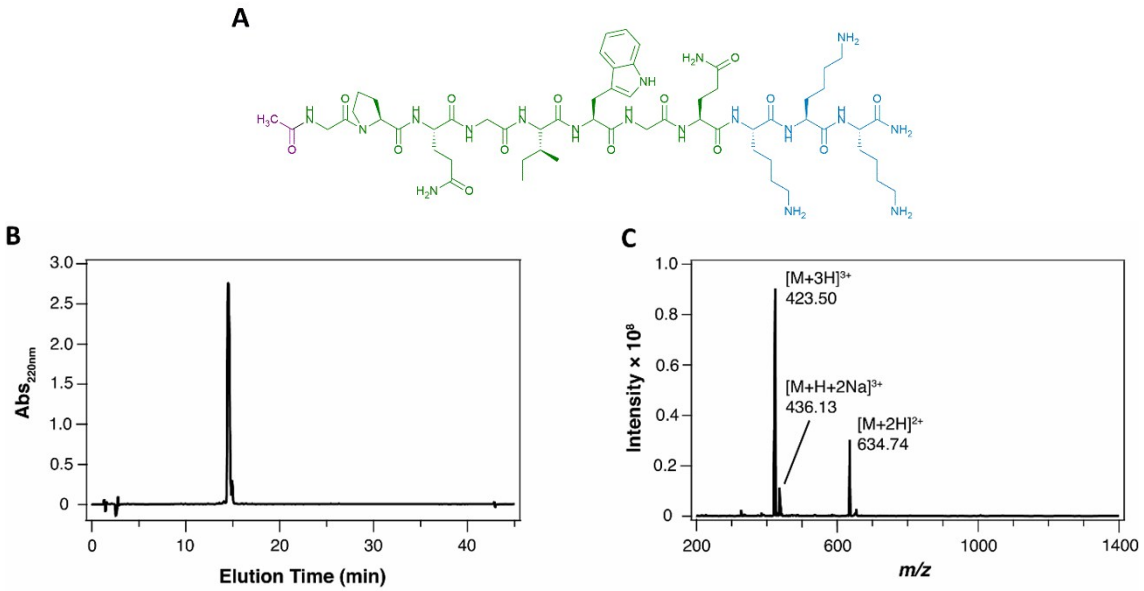

Fig. S2 Characterization of PS (CH_3CONH-GPQGIWGQKKK-$CONH_2$): (**A**) chemical structure; (**B**) analytical RP-HPLC chromatogram under the gradient of 98% to 0% H_2O (2% to 100% ACN) with 0.1% TFA from 5 to 35 min showing high purity; (**C**) ESI-MS spectrum showing the expected molecular mass ($C_{58}H_{94}N_{18}O_{14}$, Mw: 1267.49 g/mol).

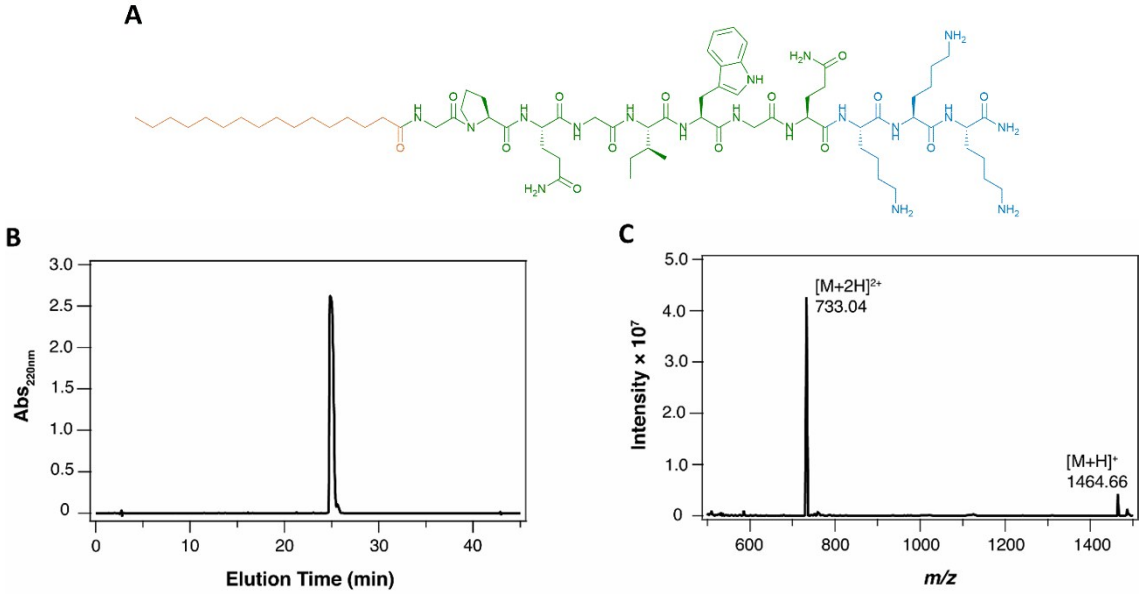

Fig. S3 Characterization of PA1 ($C_{15}H_{31}CONH$-GPQGIWGQKKK-$CONH_2$): (**A**) chemical structure; (**B**) analytical RP-HPLC chromatogram under the gradient of 98% to 0% H_2O (2% to 100% ACN) with 0.1% TFA from 5 to 35 min showing high purity; (**C**) ESI-MS spectrum showing the expected molecular mass ($C_{72}H_{122}N_{18}O_{14}$, Mw: 1463.86 g/mol).

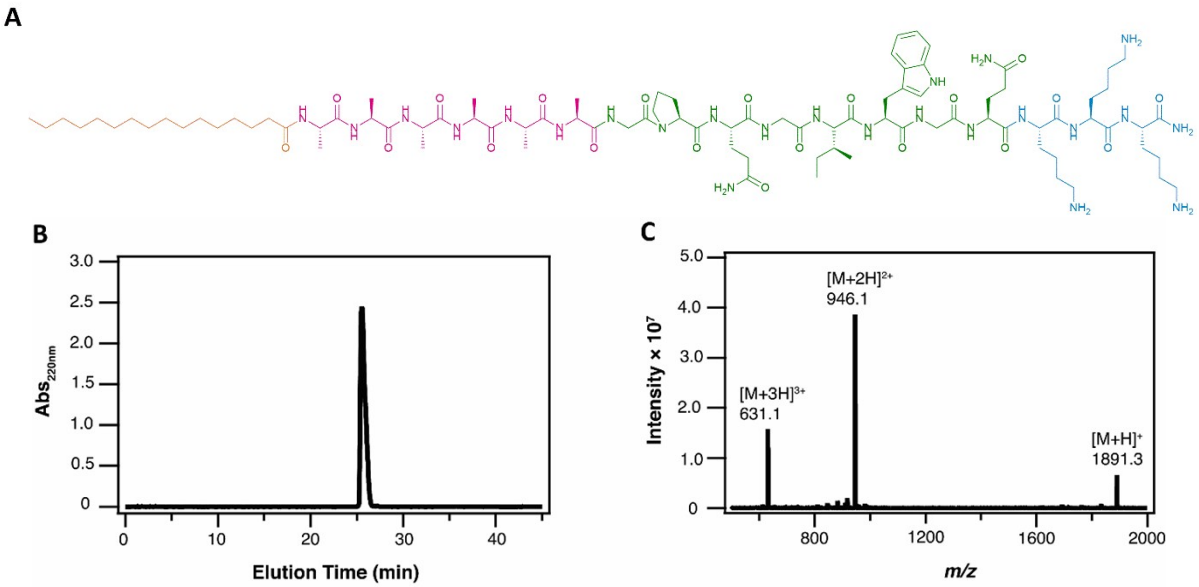

Fig. S4 Characterization of PA2 ($C_{15}H_{31}$CONH-AAAAAAGPQGIWGQKKK-$CONH_2$): (**A**) chemical structure; (**B**) analytical RP-HPLC chromatogram under the gradient of 98% to 0% H_2O (2% to 100% ACN) with 0.1% TFA from 5 to 35 min showing high purity; (**C**) ESI-MS spectrum showing the expected molecular mass ($C_{90}H_{152}N_{24}O_{20}$, Mw: 1890.33 g/mol).

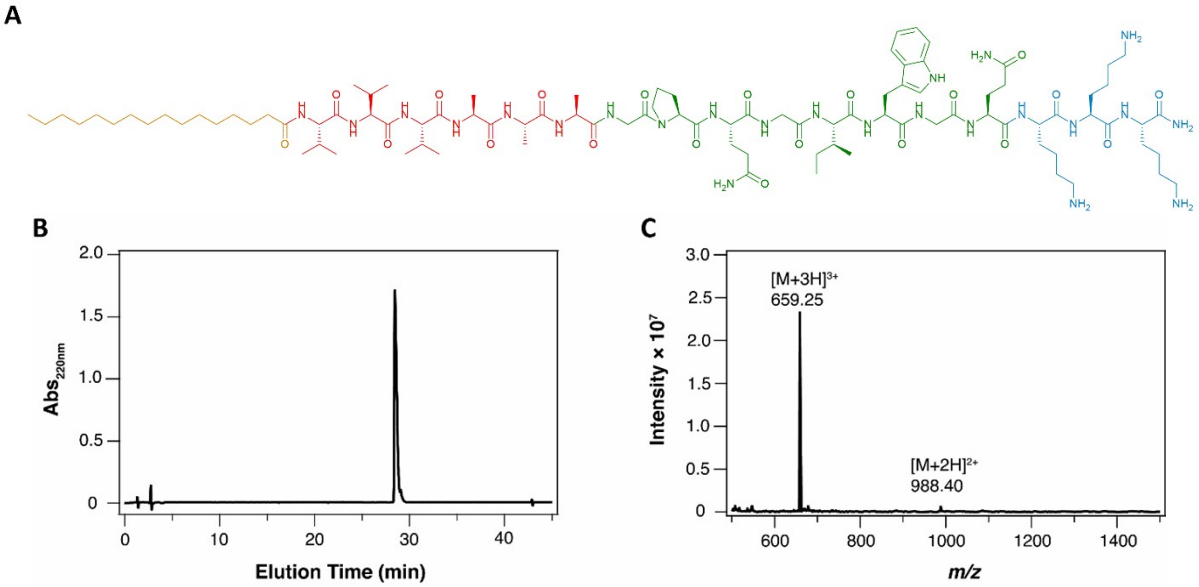

Fig. S5 Characterization of PA3 ($C_{15}H_{31}$CONH-VVVAAAGPQGIWGQKKK-$CONH_2$): (**A**) chemical structure; (**B**) analytical RP-HPLC chromatogram under the gradient of 98% to 0% H_2O (2% to 100% ACN) with 0.1% TFA from 5 to 35 min showing high purity; (**C**) ESI-MS spectrum showing the expected molecular mass ($C_{96}H_{164}N_{24}O_{20}$, Mw: 1974.49 g/mol).

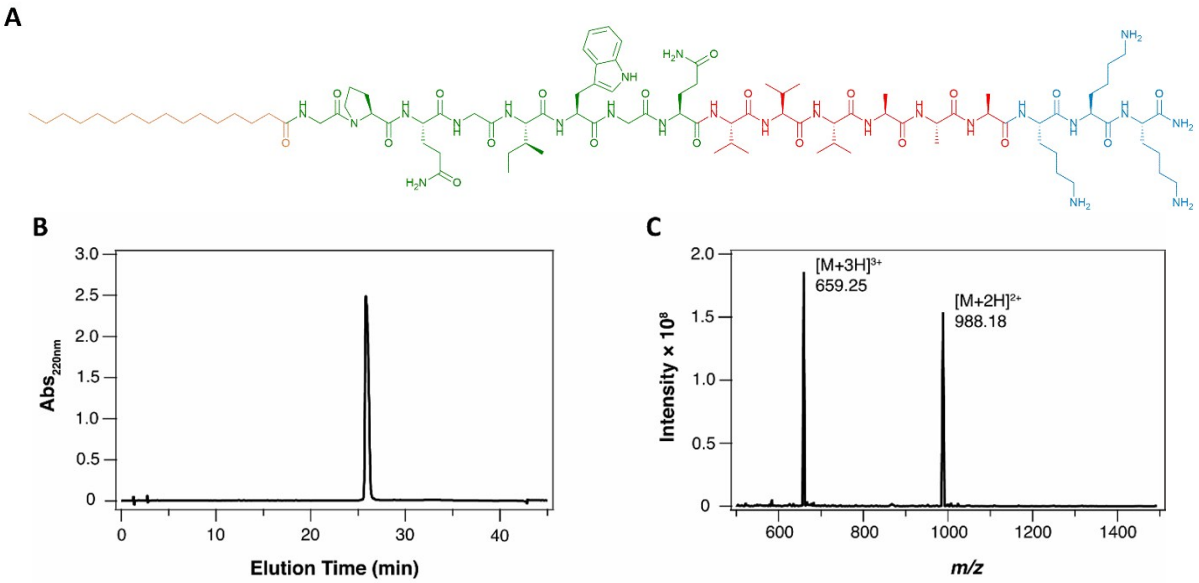

Fig. S6 Characterization of PA4 ($C_{15}H_{31}CONH$-GPQGIWGQVVVAAAKKK-$CONH_2$): (**A**) chemical structure; (**B**) analytical RP-HPLC chromatogram under the gradient of 98% to 0% H_2O (2% to 100% ACN) with 0.1% TFA from 5 to 35 min showing high purity; (**C**) ESI-MS spectrum showing the expected molecular mass ($C_{96}H_{164}N_{24}O_{20}$, Mw: 1974.49 g/mol).

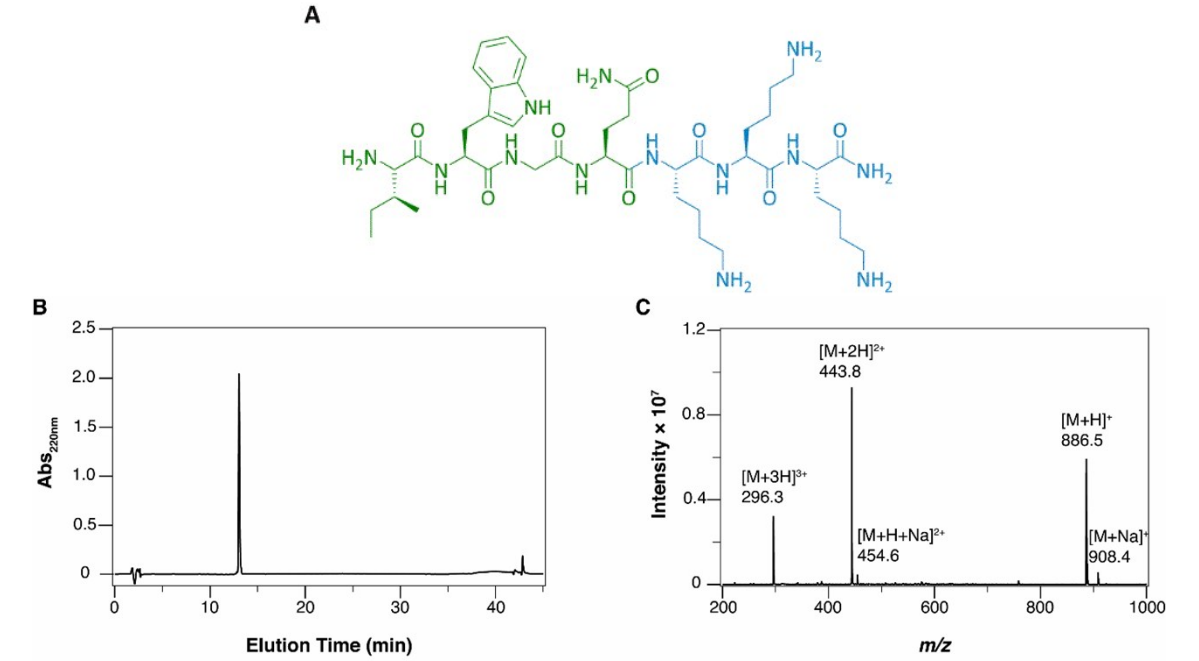

Fig. S7 Characterization of PF (NH_2-IWGQKKK-$CONH_2$): (**A**) chemical structure; (**B**) analytical RP-HPLC chromatogram under the gradient of 98% to 0% H_2O (2% to 100% ACN) with 0.1% TFA from 5 to 35 min showing high purity; (**C**) ESI-MS spectrum showing the expected molecular mass ($C_{42}H_{71}N_{13}O_8$, Mw: 886.10 g/mol).

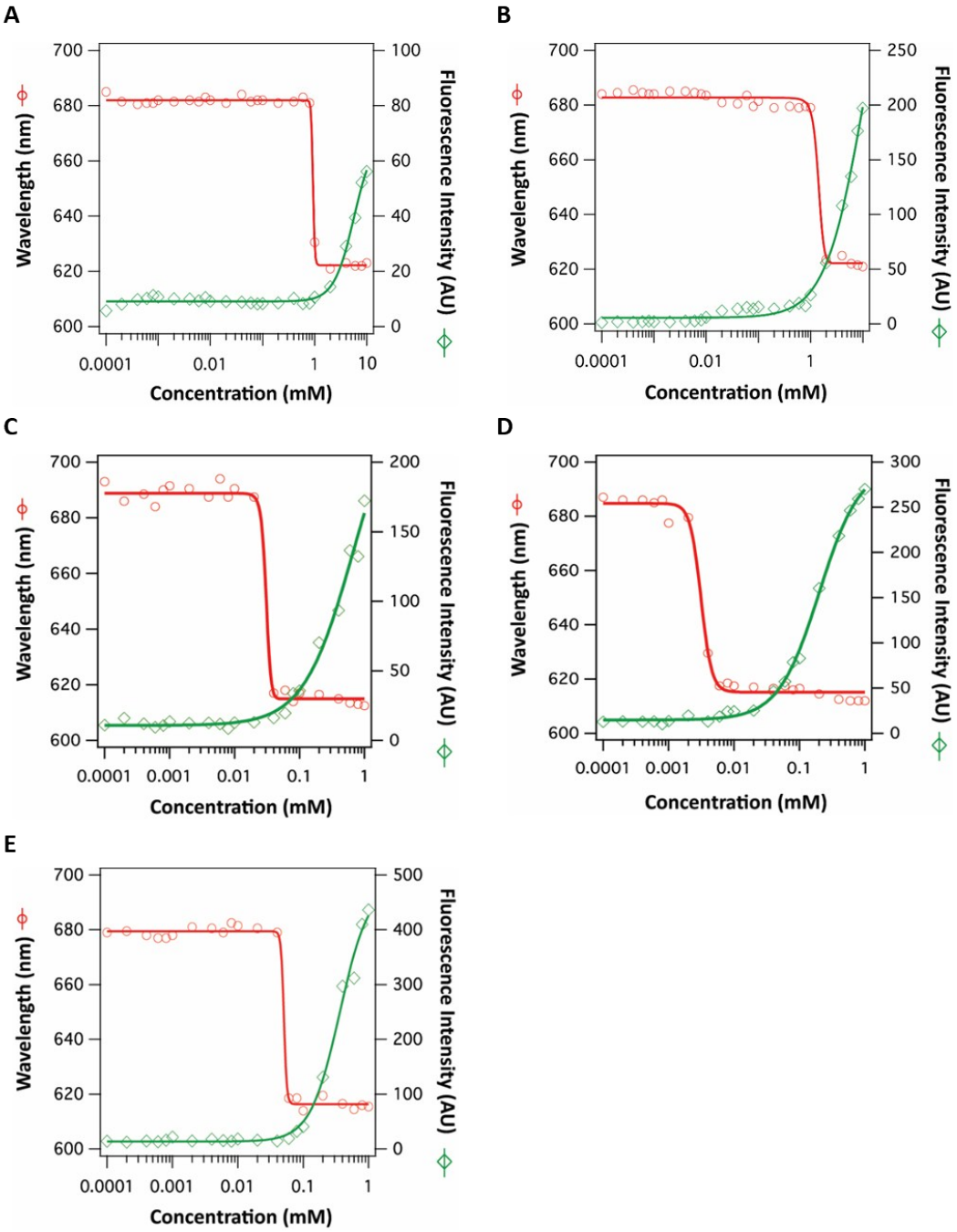

Fig. S8 CAC determination of PS and PAs: maximum fluorescence emission wavelength and intensity of nile red as function of PS and PA concentration to determine the CAC of PS at 2 mM (**A**), PA1 at 2 mM (**B**), PA2 at 0.04 mM (**C**), PA3 at 0.004 mM (**D**), and PA4 at 0.06 mM (**E**).

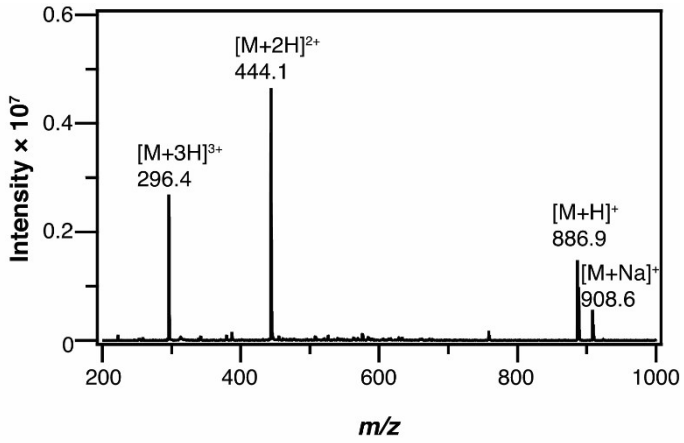

Fig. S9 Identification of the peptide fragment from MMP-1 degradation: representative ESI-MS spectrum of the fractions collected from the RP-HPLC (peak at 13 min in **Figure 4**) showing the molecular mass corresponding to the expected *N*-terminal PF (NH_2-IWGQKKK-$CONH_2$, $C_{42}H_{71}N_{13}O_8$, Mw: 886.10 g/mol).

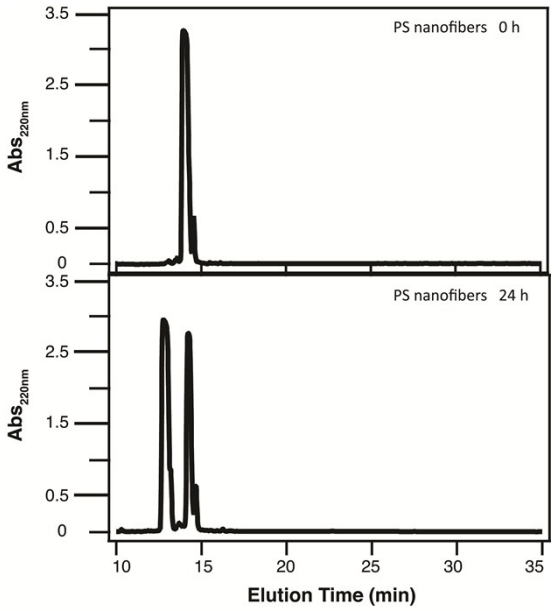

Fig. S10 MMP-1 degradation of PS nanofibers: analytical RP-HPLC traces of 5 mM PS before and after incubation with 20 nM active MMP-1 in TCNB buffer (pH 7) at 37 ^{o}C for 24 h.

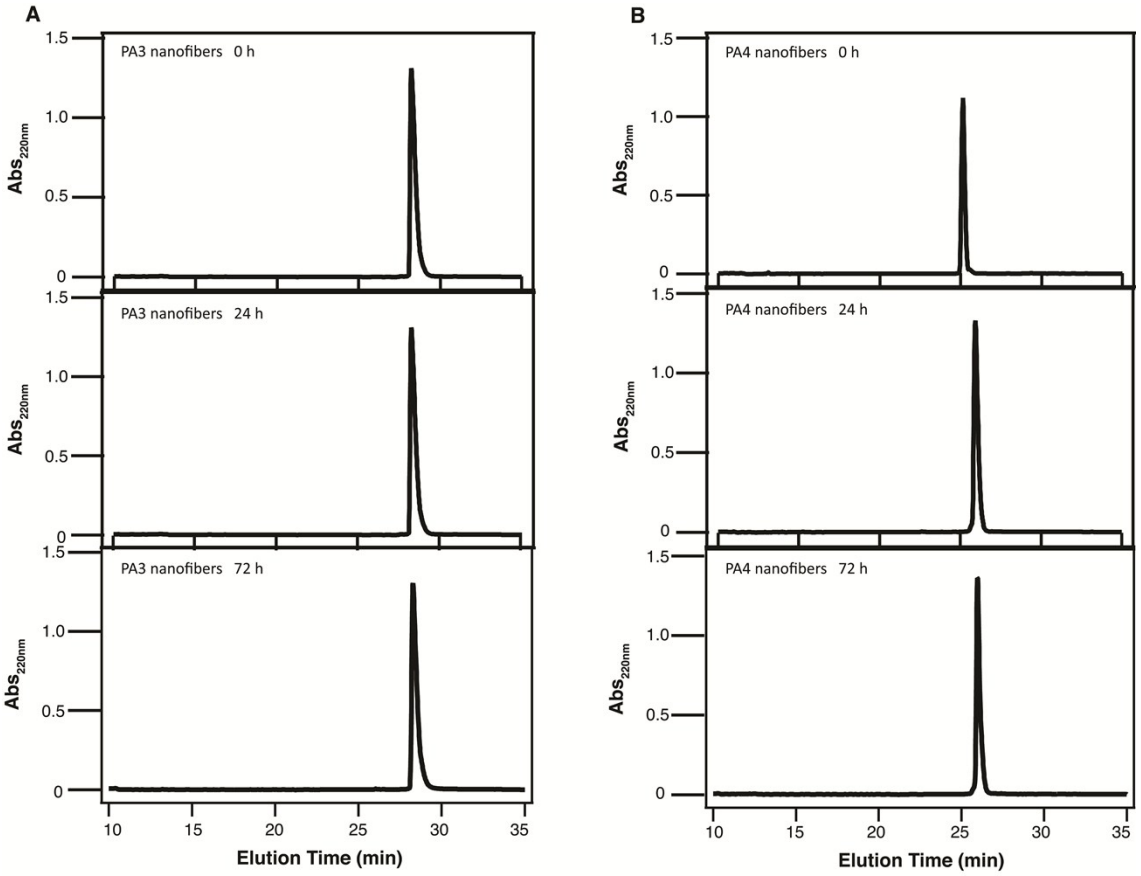

Fig. S11 MMP-1 degradation of PA3 and PA4 nanofibers: analytical RP-HPLC traces of 0.5 mM PA3 (**A**) and PA4 (**B**) before and after incubation with 20 nM active MMP-1 in TCNB buffer (pH 7) at 37 ^{o}C for 72 h.

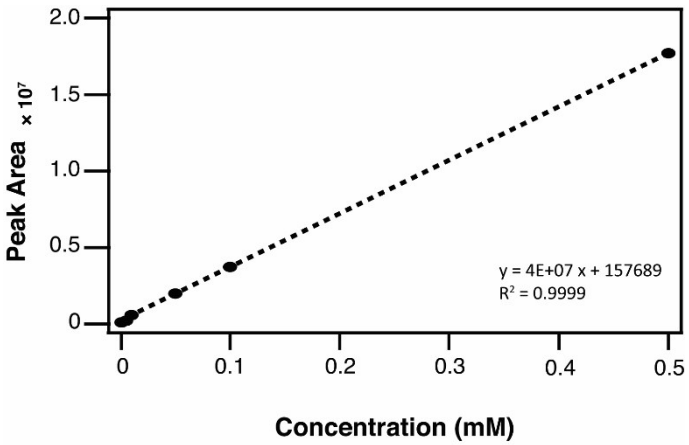

Fig. S12 Standard curve of PF: peak area of PF measured from the RP-HPLC chromatogram as function of its concentration.